ELSEVIER

Polymer 44 (2003) 1103–1115

polymer

www.elsevier.com/locate/polymer

3D Hierarchical orientation in polymer–clay nanocomposite films

A. Bafna[a], G. Beaucage[a,*], F. Mirabella[b], S. Mehta[b]

[a]*Department of Material Science and Engineering, University of Cincinnati, Mail Location 12, Cincinnati, OH 45221-0012, USA*
[b]*Cincinnati Technology Center, Equistar Chemicals LP, 11530 Northlake Dr. Cincinnati, OH 45249, USA*

Received 22 July 2002; received in revised form 30 October 2002; accepted 1 November 2002

Abstract

Organically modified clay was used as reinforcement for HDPE using maleated polyethylene (PEMA) as a compatibilizer. The effect of compatibilizer concentration on the orientation of various structural features in the polymer-layered silicate nanocomposite (PLSN) system was studied using two-dimensional (2D) small angle X-ray scattering (SAXS) and 2D wide-angle X-ray scattering (WAXS). The dispersion (repeat period) and three-dimensional (3D) orientations of six different structural features were easily identified:

(a) clay clusters/tactoids (0.12 μm),
(b) modified clay (002) (24–31 Å),
(c) unmodified clay (002) (13 Å),
(d) clay (110) and (020) planes normal to (b) and (c),
(e) polymer crystalline lamellae (001) (190–260 Å), and
(f) polymer unit cell (110) and (200) planes.

A 3D study of the relative orientation of this hierarchical morphology was carried out by measuring three scattering projections for each sample. Quantitative data on the orientation of these structural units in the nanocomposite film is determined through calculation of the major axis direction cosines and through a ternary, direction-cosine plot. Surprisingly, it is the unmodified clay which shows the most intimate relationship with the polymer crystalline lamellae in terms of orientation. Association between clay and polymer lamellae may be related to an observed increase in lamellar thickness in the composite films. Orientation relationships also reveal that the modified clay is associated with large-scale tactoid structures.

Keywords: Nanocomposites; Orientation; Small angle X-ray scattering

1. Introduction

Organically modified layered silicates have been widely studied for the past decade as property enhancers for polymeric materials. Various studies report improvement in mechanical [1–3], thermal [4,5], flammability [4,5], and barrier [6,7] properties of thermoplastics by addition of organically modified layered silicates to polymer matrices. These modified thermoplastic systems are called polymer-layered silicate nanocomposites (PLSN). Due to this property enhancement at low filler content (2–6 wt%), PLSN systems have drawn tremendous attention. In general these PLSN systems possess several advantages including; (a) they are lighter in weight compared to conventionally filled polymers due to property enhancement even at small clay loadings; (b) they exhibit outstanding barrier properties without requiring a multi-layered fabrication, allowing for recycling.

PLSN systems are made of two components; the base resin, and a modified layered silicate (clay). A potential third component is a compatibilizer. Modified layered silicates are composed of silicate layers that can intercalate organic polymer chains if appropriate ionic or hydrogen bonding groups are present on the polymer. For example, montmorillonite is a 2:1 type layered silicate and is the most commonly used filler in PLSN systems [8]. 2:1 layered silicates are composed of an octahedral alumina or magnesia sheet sandwiched between two tetrahedral sheets of silica. The silica sheets have Na^+, Ca^{2+}, or K^+ ions on their surfaces. The combined thickness of the two silica and one alumina or magnesia sheet is about 0.95 nm [8]. The presence of positive ions on the surface of the silica sheets increases the *d*-spacing in the normal (002) direction of the clay platelet which generally varies from 1.0 to 1.3 nm. The presence of positive ions on the surface also makes the clay

* Corresponding author. Tel.: +1-513-556-3063; fax: +1-513-556-2569.
E-mail address: beaucag@uc.edu (G. Beaucage).

0032-3861/03/$ - see front matter © 2002 Elsevier Science Ltd. All rights reserved.
PII: S0032-3861(02)00833-9

platelet hydrophilic and thus incompatible with many polymers. The organophilicity of the clay platelets can be increased by exchange of these ions with organic cations (alkyl ammonium ions) [9,10]. Ion exchange and surfactant treatment are not absolutely effective in commercially modified clay. Generally, two clay species might result: unmodified clay with small layer spacing on the order of 1 nm, and onium (alkyl ammonium) modified clay with a layer spacing on the order of 1–5 nm depending on the number of carbon atoms in the chain of the onium ion [8]. For the commercially modified montmorillonite studied here, about one-third of the clay remains with unmodified spacing as discussed below. The onium modified clay is thought to retain planar 0.95 nm thick aluminosilicate trilayers. The main evidence for this comes from the existence of a stacking period after intercalation and X-ray reflection from in-plane crystallographic structure. Two diffraction peaks are generally observed from these trilayer structures; (a) a 'long-period'-like layer spacing, (002), oriented normal to the layer face, and (b) a weaker (110)/(020) combined orthogonal reflection at about 0.44 nm. The 0.44 nm reflections should always orient orthogonal to the layer spacing peak for planar aluminosilicate trilayers [11].

For the greatest property enhancement in PLSN systems it is generally believed that the clay layers should disperse as single trilayer (0.95 nm) platelets throughout the polymer matrix, exfoliation. To attain such dispersion of clay platelets the polymer should first penetrate between the clay platelets. This intercalation is possible if the polymer and the clay surfaces are compatible. Depending on the interaction between the clay and the polymer, and the clay loading [12,13] different regimes of dispersion are expected. If the polymer just enters between the clay platelets the system is said to be intercalated. Some models predict a nematic phase for the platelets with polymer chains co-planar to the trilayers [12,13]. Intercalation increases the *d*-spacing of the clay platelets by around 0.5–1.5 nm, a distance associated with a polymer monolayer [12,13]. Exfoliated systems are formed when the polymer enters between the clay platelets and force them apart so they no longer interact with each other. This condition is modeled as a low concentration limit for relatively weakly-interacting systems [12,13].

Recent studies [14–16] mention that along with exfoliation, orientation of the clay platelets plays a major role in tuning some property enhancements in PLSN systems. For example, the effect of shear on the orientation of the clay platelets and the polymer unit cells in PLSN systems has been studied [11,17–21]. In some cases three-dimensional (3D) orientation of clay platelets and unit cells in polymer nanocomposites have been studied [15,16,20,21].

PLSN's are generally composed of a collage of interacting structural features. On the nanoscale, polymer crystallites in the form of lamellar sheets of about 5–10 nm thickness coexist with the 1–2 nm thick clay platelets. Both the clay platelets and the polymer lamellae prefer to stack, especially at high volume fractions [22]. In studies on preferential orientation of clay platelets and polymer crystallites in nylon–clay nanocomposite films, Kojima et al. [20] observed that both clay platelets and polymer crystallites align parallel to the surface of the film and along the flow axis (machine direction). In injection molded nylon–clay nanocomposite samples, Kojima et al. [21] found that the polymer crystallites either align parallel (high shear region) or perpendicular (low shear region) to the clay platelets. Contrary to Kojima's observation, Vaia et al. [11] observed that polymer crystallites align perpendicular to the clay platelets in nylon–clay electrospun fibers where exceedingly high elongational strain rates are expected. Varlot et al. [15] observed that in intercalated nylon–clay nanocomposites, the clay platelets aligned with normals both parallel and perpendicular to the thickness of an injection molded sample consistent with Kojima et al. [21]. Although it is clear that the polymer lamellae align in different directions depending on the type of deformation, the cumulative strain and the strain rate, the relationship of clay platelet orientation to the orientation of other structural units, such as the polymer unit cells and polymer lamellae still remains unclear. Most of literature studies use nylon-6 as the base resin. Nylon, being a polar polymer, disperses clay platelets without addition of compatibilizer. On the other hand polymers like polyethylene (PE) and polypropylene (PP) are non-polar in nature, so are not compatible with modified clays. For these systems, the loading of compatibilizer becomes an important parameter. Orientation of clay platelets and polymer lamellae are expected to depend on clay loading, polymer degree of crystallinity, the enthalpic interaction between the clay surface and polymer, as well as polymer chain flexibility and molecular weight in addition to the accumulated shear strain and rate of strain and type of deformation.

PE is one of the most important commodity polymers with a worldwide consumption of about 44 million metric tons/year [23]. A large portion of the polyethylene produced is consumed in the film market. Due to its low cost, high-density polyethylene (HDPE) is increasingly finding acceptance as a wrapping material for food products. HDPE is known to have poor barrier properties for gases, organic solvents and hydrocarbons [24,25]. Reports on enhancement of barrier, mechanical and thermal properties on addition of clay to a polymer have opened new fields of research in the polyolefin industry. As mentioned earlier, polyolefins being non-polar show poor compatibility with modified clays. Various authors [1,26–28] reported on the dispersion of clay platelets in polyolefins by addition of a compatibilizer such as maleated polypropylene or maleated polyethylene. The compatibilizer is generally believed to first enter between the clay platelets, separate the clay trilayers and increase the gallery height facilitating intercalation of the non-polar polymer. This could be advantageous as strong clay/polymer interactions are believed to favor intercalation over exfoliation [12]. Although previous

studies showed the effect of compatibilizer on property enhancement in polyolefin nanocomposites, the literature lacks a clear picture of the effect of compatibilizer on the orientation/dispersion of the clay platelets and the effect of this clay orientation on the orientation of other structural units such as polymer unit cells and polymer lamellae. Moreover, all the orientation studies mentioned above provide only qualitative data on orientation and little quantitative data are available in the literature concerning the relative orientation of structures in these systems.

In this study two HDPE–clay nanocomposite films cast from the melt (that is extruded from a coat-hanger die to form a film) were investigated. Organically modified clay was used as reinforcement while maleated polyethylene (PEMA) was used as compatibilizer. Various studies [1, 3–6] report improvement in properties of polymers by addition of 2.5–5% organically modified layered silicates to polymer matrices. Oya et al. [3] observed that the intensity of the diffraction peak from clay was weak due to lower content of montmorillonite (3%) in the nanocomposite. In our earlier studies (not published) the properties of polyethylene nanocomposites were found to monotonically increase with increasing clay loading up to 6–8 wt%. Thus in order to enhance scattering from clay in both small angle X-ray scattering (SAXS) and WAXS, the concentration of clay was chosen to be 6% by weight in this study. The concentration of clay was kept constant for two films while the compatibilizer concentration was varied. The effect of compatibilizer concentration on the orientation of various structures in the PLSN system was studied using two-dimensional (2D) SAXS and 2D wide-angle X-ray scattering (WAXS) in three sample/camera orientations. Reflections and orientation of six different structural features were easily identified:

(a) clay clusters/tactoids (0.12 μm),
(b) modified/intercalated clay stacking period (002) (24–31 Å),
(c) stacking period of unmodified clay platelets (002) (13 Å),
(d) clay (110) and (020) planes, normal to (b) and (c),
(e) polymer crystalline lamellae (001) (190–260 Å), long period[1] and
(e) polymer unit cell (110) and (200) planes.

The corresponding reflections are identified in Fig. 2 as discussed below. A 3D study of the relative orientation of all the above mentioned structures was carried out by measuring three projections for each sample. Quantitative data on the orientation of these structural units in the nanocomposite film is determined through calculations of the major axis direction cosines and through a ternary, direction-cosine plot called a 'Wilchinsky triangle' [29–32] previously proposed in lamellar orientation studies [30]. It allows a direct comparison of average preferred orientation for different structural features. In this way it is conceptually more useful than stereographic projections involving orientation density maps for a single X-ray reflection, pole figure.

[1] Chain tilt effects are discussed below, (001) is an average crystallographic direction.

2. Experimental and analysis

2.1. Material

Films designated HD000, HD603 and HD612, cast (extruded into a thin sheet) under similar conditions at Equistar Technology Center (Cincinnati, OH) were studied. The films were designated as HDXYY, where 'HD' is high density polyethylene, 'X' is wt% of the montmorillonite and 'YY' is wt% of the compatibilizer. High density polyethylene (density = 0.96 g/cc, molecular weight = 140,000 g/mole and polydispersity index $M_W/M_N = 6.6$) was used as the base resin. Weight fractions were calculated based on the total mass of the composite. Maleated-polyethylene (PEMA, 2% maleic anhydride content) was used as the compatibilizer. Natural montmorillonite modified with a quaternary ammonium salt was used as reinforcement. The film designated HD000 had no clay or compatibilizer in it. The clay concentration (6 wt%) was kept constant in both HD603 and HD612. The mass ratio of clay to compatibilizer was 2:1 for HD603 and 1:2 in HD612. The final compositions and properties of the three films are shown in Table 1.

The polymer and clay were mixed together and extruded into thin strands using a ZSK-30 twin screw extruder. The screw speed was 250 rpm and the temperature in the barrel varied from 180 to 190 °C and was 180 °C in the die. The strands were then pelletized. The dried pellets of the two nanocomposites and the base resin were cast into films of 2 mil (50 μm) thickness using an extruder fitted with a film casting die (die gap = 50 mil). The temperature in the extruder varied from 170 °C in zone-1 to 185 °C in zone-3 and was 175 °C in the die. After extrusion, the films were quenched over chilled rolls. The degree of crystallinity and melting point of the films was measured using a Perkin–Elmer DSC-7. The melt index was obtained in accordance to ASTM D1238 using an extrusion plastometer.

2.2. Ultra-small angle X-ray scattering (USAXS) measurements

The sizes of clay tactoids were determined using a USAXS camera at UNICAT facility at APS using ID-33 beamline (www.aps.anl.gov). Desmeared USAXS data was fitted using the unified function to yield R_g which was converted to a mean thickness using a platelet approximation, $t_{platelet} = 2R_g$ [33,34]. This mean size and plate-like

Table 1
Compositions and properties of the three films. L from SAXS, T_m and X_c from DSC, and MI from an extrusion plastometer (melt flow indexer). T_m, melting point; X_c, degree of crystallinity normalized by the polymer weight fraction; L, polymer lamellar long period; l_c, polymer lamellar thickness, LX_c

Sample	Clay (wt %)	Compatibilizer (wt%)	Base resin (wt %)	MI (g/10 min)	T_m (°C)	X_c (%)	L (Å)	l_c (Å)
HD000	0	0	100	2.06	133	80	212	169
HD603	6	3	91	1.25	132	79	256	201
HD612	6	12	82	0.75	132	78	256	198

structure of the tactoids were verified using transmission electron microscopy (TEM).

2.3. Simultaneous 2D small angle and 2D wide angle X-ray scattering (SAXS and WAXS)

2.3.1. SAXS and WAXS measurements

SAXS measurements were conducted on a pinhole geometry camera using a 2D wire detector at 1 m sample to detector distance. WAXS measurements were conducted on the same camera with an image plate detector placed 5 cm from the sample. X-rays from a 12 kW Rigaku rotating anode generator were passed through a nickel filter to remove the Cu Kβ X-rays, but the beam was polychromatic to some extent. The wire detector used for SAXS allowed energy resolution to 1.54 Å (Cu Kα but the image plate had no energy resolution leading to some smearing of the data as evidenced in the azimuthal curves presented later (e.g. Fig. 6). For this reason SAXS and WAXS curves cannot be quantitatively compared one to one. Within the WAXS patterns, peaks are subjected to the same smearing effect allowing a one to one comparison. SAXS orientation values are more accurate and some reflections overlap in the data from the two cameras allowing an assessment of the smearing in WAXS due to wavelength dispersion.

The 2D measurements are useful in determining both size and relative orientation of various structural components in the film. Because the films were very thin (50 μm); around 30–50 films were stacked over one another for measurement. Care was taken that the films were stacked in such a manner that all the films in a stack had their machine direction (MD), transverse direction (TD) and normal direction (ND) aligned. Stacks of approximately 2 mm thickness were prepared from the 50 μm films.

2.3.2. SAXS and WAXS analysis

In order to study the 3D orientation of various structures in the film, X-ray measurements need to be carried out for at least two orientations of the sample with respect to the X-ray beam. A third orientation can serve as a crosscheck for 3D orientation. Projections are designated by the three principal sample axes, M, machine direction, T, transverse direction and N, normal direction. Fig. 1 shows the three sample orientations used for the SAXS and WAXS measurements. Corrected 2D SAXS and WAXS patterns for the different orientations are shown in Fig. 2. The sample orientations are designated with reference to Fig. 1.

For the MT and MN orientations, the azimuthal average of the 2D patterns (Fig. 2) yields the radial plots in Fig. 3(a) and (b), showing the intensity versus scattering vector $q = 4\pi[\sin(\theta/2)]/\lambda$, where θ is the scattering angle and $\lambda = 1.542$ Å is the wavelength. The d-spacing is calculated using Bragg's law, $d = 2\pi/q^*_N$, where q^*_N is the value of q at maximum intensity in a Lorentizian corrected SAXS pattern of Iq^2 versus q (not shown). The radial plots obtained from the SAXS and WAXS measurements give data on periodicity (dispersion) of (a) clay tactoids, (b) modified/intercalated clay platelets, (c) unmodified clay platelets, (d) clay (110) and (020) planes, (e) polymer lamellar, and (f) polymer unit cell (110) and (200) planes.

For the MT and MN orientations the radial average of the 2D patterns yield the azimuthal plots in Fig. 4, showing intensity as a function of azimuthal angle (f). For each sample orientation, azimuthal plots for intercalated clay, unmodified clay, polymer lamellar and polymer unit crystals can be made. Fig. 4(a) compares the orientation data obtained from SAXS for the intercalated clay platelets in HD603 and HD612. Fig. 4(b) compares orientation data obtained from SAXS and WAXS for unmodified clay (002), intercalated clay (002), polymer lamellae (002) and polymer

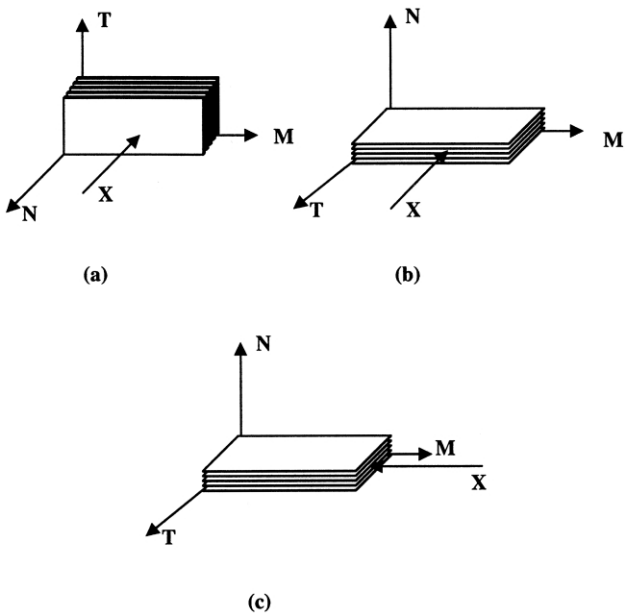

Fig. 1. Different orientations of the film: (a) MT orientation, (b) MN orientation, and (c) NT orientation. X indicates direction of the X-ray beam.

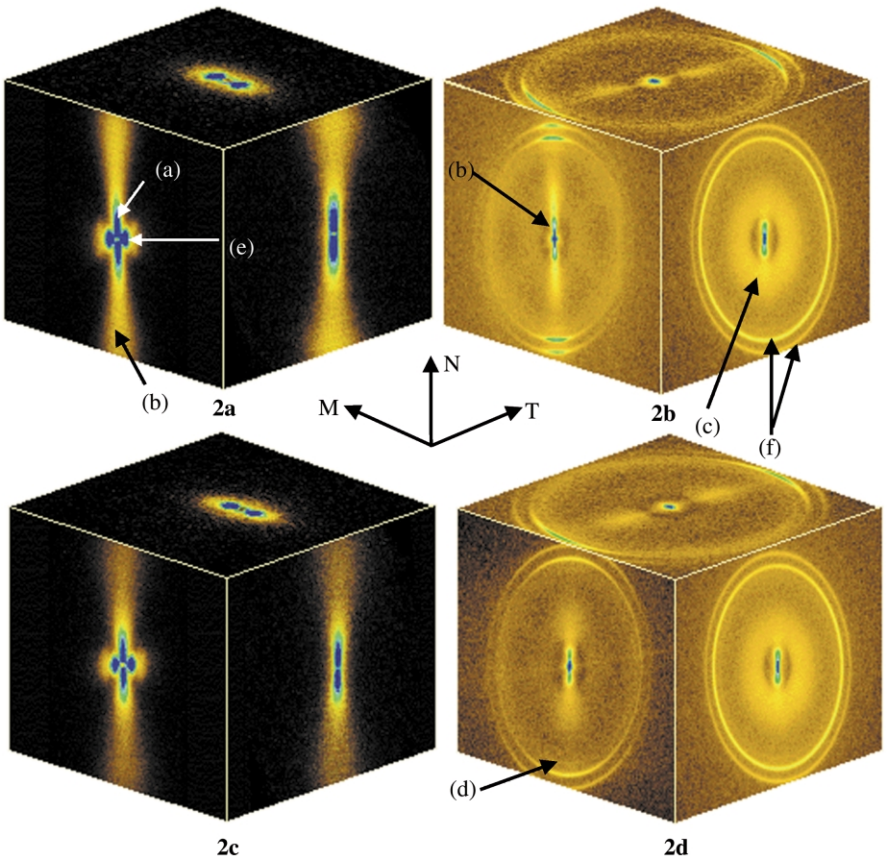

Fig. 2. 2-D SAXS ((a) and (c)) and WAXS ((b) and (d)) patterns for orientation MN (left face), NT (right face) and MT (top face) of films HD603 ((a) and (b)) and HD612 ((c) and (d)). The numbers in the parenthesis represent the reflections from the following: (a) clay tactoids, (b) modified/intercalated clay (002) plane, (c) unmodified clay (002) plane, (d) clay (110) and (020) plane, (e) polymer crystalline lamellar, (f) polymer unit cell (110) plane (inner ring) and (200) plane (outer ring).

unit cell (110) planes in HD612. For any periodic structure, the sharpness of the azimuthal peak reflects the extent of orientation of the structural normal. The polymer lamellae curve has been truncated owing to the bright anisotropic streak associated with tactoids at 90 and 270° (Fig. 2) as noted in the caption. This truncation has little effect on the calculation of orientation, discussed below, since the squared azimuthal cosine value is low at these angles and the intensity associated with the lamellar long period is at its lowest point.

The azimuthal plot (Fig. 4) can be used to calculate the average cosine square of the normal to the plane of reflection [30] for the particular projection. For example, the MT planar projection, $\langle \cos^2 \phi_{MT} \rangle$, can be calculated by,

$$\left\langle \cos^2(\phi_{MT}) \right\rangle = \frac{\int_0^{2\pi} I(\phi_{MT}) \cos^2(\phi_{MT}) \mathrm{d}\phi_{MT}}{\int_0^{2\pi} I(\phi_{MT}) \mathrm{d}\phi_{MT}} \quad (1)$$

The ϕ_{MT} value from orientation 1 is used along with ϕ_{MN} value from orientation 2 to determine the 3D orientation of the structural normals in the three principle film axes represented by ϕ_M, ϕ_T and ϕ_N.

Eq. (1) involves subtle assumptions concerning the orientation distribution in the sample. The basic assumption involved in the approach is that there is a distribution of orientation and that the population of orientations can be represented by a single average direction of orientation in 3D space. Symmetry of the SAXS or WAXS reflections about the beam center, Fig. 2, serves as support for the appropriateness of this assumption. The assumption is generally good for small angle scattering. Additionally, the polychromaticity of the WAXS pattern, discussed above, improves on this assumption in the WAXS regime.

2.3.3. SAXS and WAXS calculations

Fig. 5 schematically shows the three observed projections and orientation angles obtained from Fig. 4 using Eq. (1) as well as the 3D orientation of the structural normal vector from the scattering, **q**. The following equations are used to calculate ϕ_M, ϕ_T and ϕ_N from ϕ_{MT} and ϕ_{MN} [30]. Using Fig. 5(a),

$$q_M = q_{MT} \cos \phi_{MT} = q \cos \phi_M \quad (2)$$

$$q_T = q_{MT} \sin \phi_{MT} \quad (3)$$

Similarly, from Fig. 5(b),

$$q_M = q_{MN} \cos \phi_{MN} \quad (4)$$

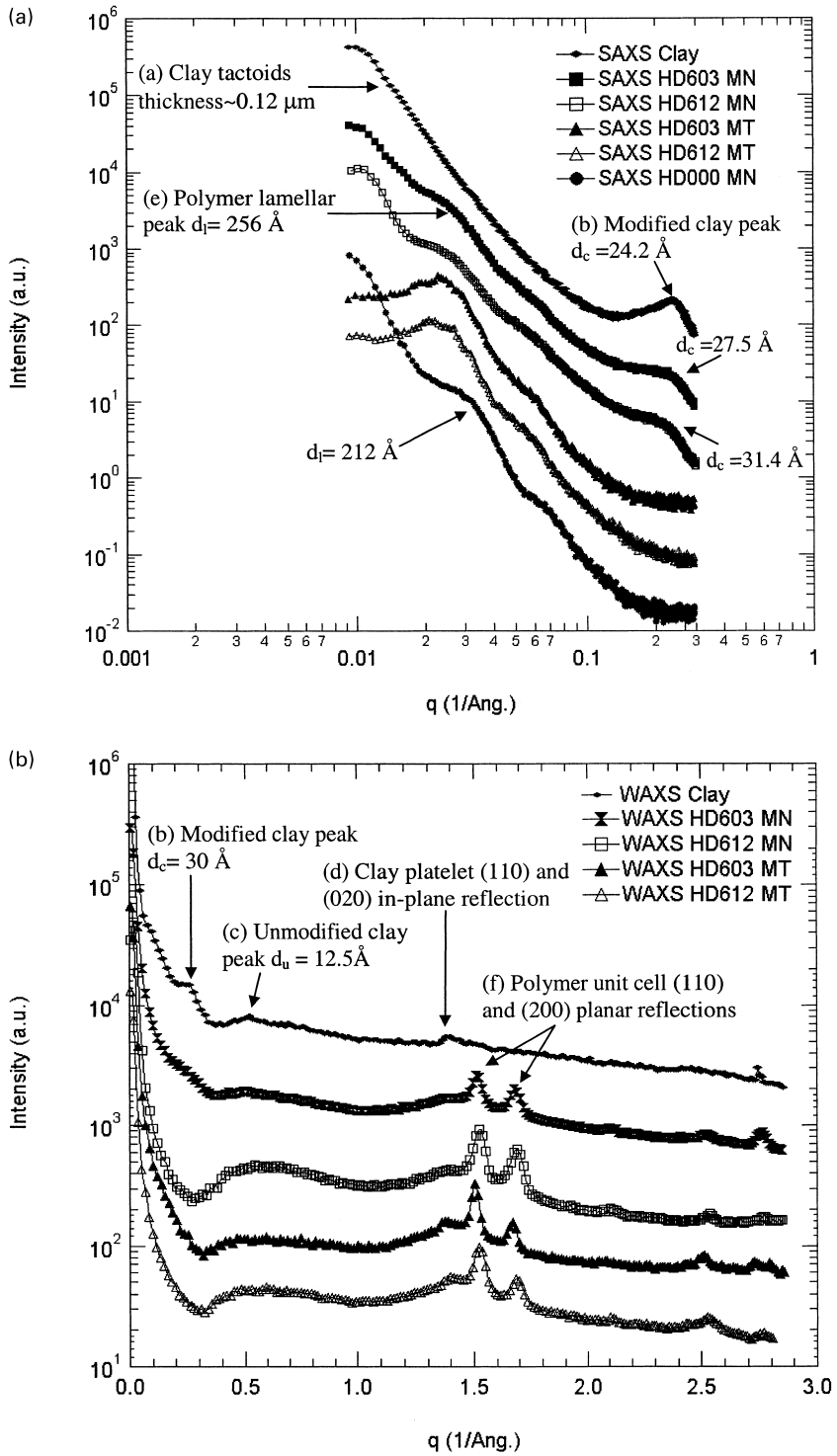

Fig. 3. (a) SAXS log–log radial plots for clay and HD603, HD612 and HD000 in orientation MN and MT. Here d_c represents the d-spacing of the intercalated/modified clay while d_l represents the d-spacing of the polymer lamellar structures in the nanocomposite. (b) WAXS log–linear radial plots for clay and the two films in orientation MT and MN. Here d_u represents the d-spacing of the unmodified clay in the nanocomposite.

$$q_N = q_{MN} \sin \phi_{MN} \quad (5)$$

From Eqs. (2)–(5),

$$q_T/q_M = \tan \phi_{MT} \quad (6)$$

$$q_N/q_M = \tan \phi_{MN} \quad (7)$$

$$q_N/q_T = \tan \phi_{MT}/\tan \phi_{MT} \quad (8)$$

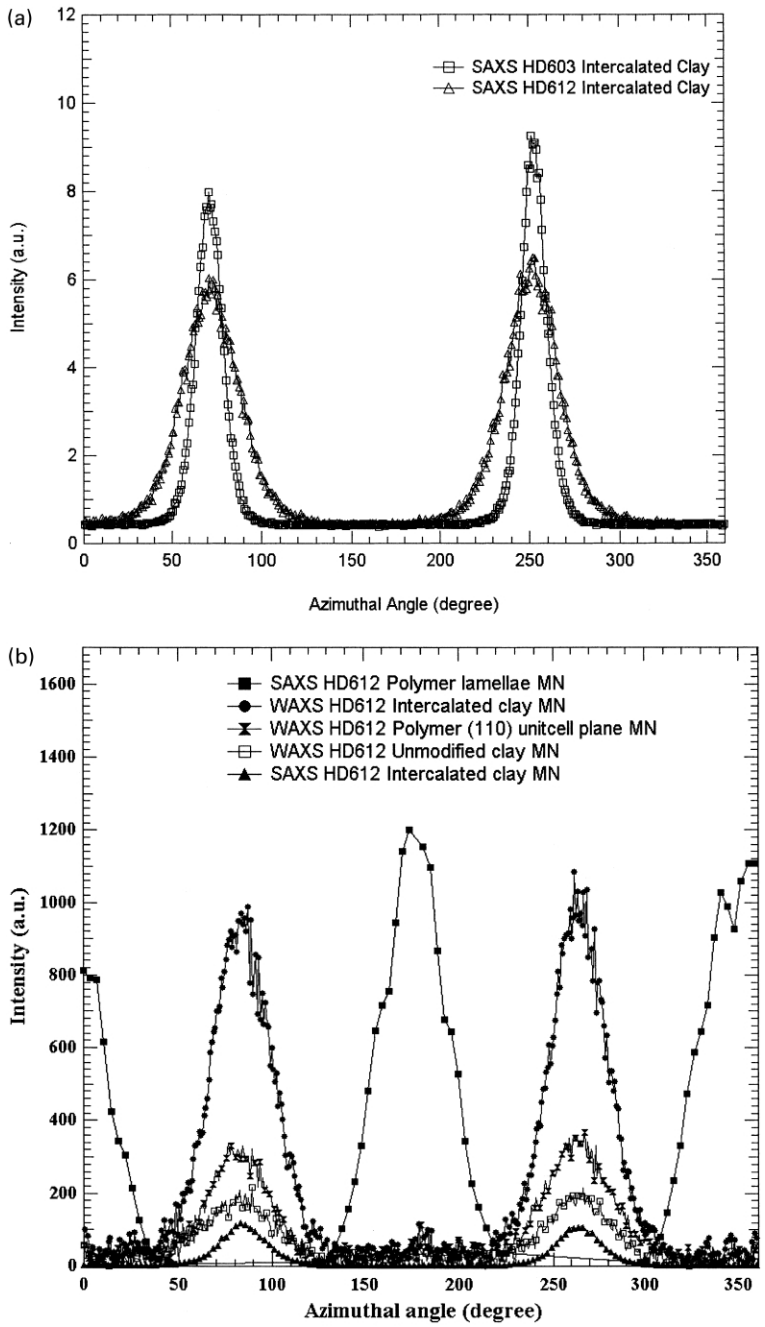

Fig. 4. (a) Azimuthal plot showing the orientation of intercalated clay platelets in HD603 and HD612 in film MN orientation (data averaged from $q = 0.15$–0.30 Å^{-1}). (b) Azimuthal plot showing orientation of unmodified clay, intercalated clay, polymer lamellae and polymer unit cell (110) plane in HD612. The polymer lamellae curve has been truncated owing to the bright anisotropic streak associated with tactoids at 90 and 270° (Fig. 2) as discussed in the text.

From Fig. 5,

$$\cos^2\phi_M = q_M^2/q^2 = q_M^2/(q_M^2 + q_N^2 + q_T^2) \quad (9)$$

$$\cos^2\phi_N = q_N^2/q^2 = q_N^2/(q_M^2 + q_N^2 + q_T^2) \quad (10)$$

$$\cos^2\phi_T = q_T^2/q^2 = q_T^2/(q_M^2 + q_N^2 + q_T^2) \quad (11)$$

Substituting Eqs. (6)–(8) in Eqs. (9)–(11) and substituting $A = \tan\phi_{MN}$ and $B = \tan\phi_{MT}$

$$\cos^2\phi_M = 1/(1 + A^2 + B^2) \quad (12)$$

$$\cos^2\phi_N = A^2/(1 + A^2 + B^2) \quad (13)$$

$$\cos^2\phi_T = B^2/(1 + A^2 + B^2) \quad (14)$$

In this way values of ϕ_{MT} and ϕ_{MN} yield the values of $\cos^2(\phi_M)$, $\cos^2(\phi_T)$ and $\cos^2(\phi_N)$ reported in Table 2. These $\cos^2(\phi_i)$ values are numerically derived from the mean values of the type value $\langle\cos^2(\phi_{MN})\rangle$ and represent a type of average value.

The average cosine square projection of the structural

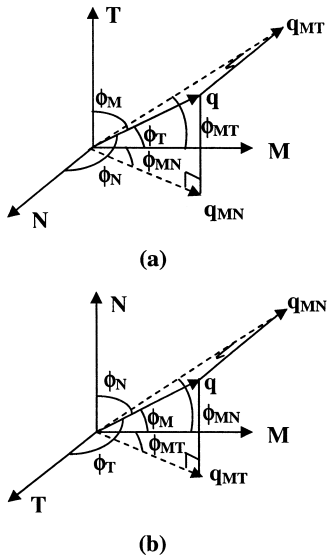

Fig. 5. Direction of scattering vector q in two different orientations, (a) Orientation MT: q_{MT} is the projection of the scattering vector q on the MT plane while ϕ_{MT} is the angle made by the scattering vector with the horizontal (MD) when projected on the MT plane, and (b) Orientation MN: q_{MN} is the projection of the scattering vector on the MN plane while ϕ_{MN} is the angle made by the scattering vector q with the horizontal (MD) when projected on the MN plane. Dashed lines represent projection of the scattering vector on the respective planes.

normals from the i axis, $\cos^2\phi_i$, can be used in a Wilchinsky triangle [29–32] (Fig. 6). This ternary plot graphically displays the average 3D direction of the structural normal orientation with a single point. The Wilchinsky triangle is constructed by counting from the opposite side of a direction i the value of $\cos^2\phi_i$ and making a point where the three $\cos^2\phi_i$ values intersect. For a randomly oriented sample $\cos^2\phi_M = \cos^2\phi_N = \cos^2\phi_T = 1/3$ and a point in the center of the Wilchinsky triangle results. For perfect orientation of a plane in MT the normal points in the N direction and a point at the ND corner results. Any line in the Wilchinsky triangle reflects a planar projection [30]. An orientation of a plane normal to the MT plane occurs for a point on the MT axis. The length of a line from a given orientation to the random point is a measure of the orientation of a structure. The orientation in a planar projection such as the MT plane is determined from the Wilchinsky plot by projecting a line from N to the MT axis through the structural point on the Wilchinsky triangle.

One assumption of the orientation analysis presented above is that the orientation density, such as plotted in a pole figure, can be represented by a single average direction. For the samples studied here this assumption is appropriate and allows for a direct comparison of average orientation over wide range of structural size, 10 μm to 1 Å. (We are working on adaptations for fiber patterns where bimodal orientation distributions are observed.)

3. Results and discussion

Natural (unmodified) montmorillonite is known to have a d-spacing of 10–13 Å, while organically modified clay has a d-spacing of 15–30 Å [8]. The WAXS radial plots (Fig. 3(b)) for pure clay show two peaks at $q = 0.26$ and 0.51 $Å^{-1}$ corresponding to a d-spacing of 24.5 and 12.5 Å. This indicates that both modified and unmodified clay species were present in the clay. Depending on the film projection and orientation, a correlation peak may broaden or even completely disappear in the radial plots (Fig. 3(a), $q = 0.24$ $Å^{-1}$ for filled markers (HD603)). This shows that, due to orientation, a single projection can be a misleading measure of clay platelet dispersion for instance. The dimensions of the clay tactoids (thickness ~0.12 μm and lateral width ~1.6 μm) were obtained using unified fits [33,34] to ultra SAXS data on the films using the UNICAT beamline at the Advanced Photon Source, Argonne National Laboratory, Illinois. In SAXS and WAXS radial plots, clay tactoids do not display a discrete peak, associated with spatial correlation, since they are not periodic structures. Although the clay tactoids don't show a discrete peak in the radial plot (Fig. 3(a)), they are seen to be close to planar structures (2D) with a mass fractal dimension (d_f) of 2.4 in USAXS data (not shown). The orientation data was obtained by analyzing the intensity for a range of q values from 0.015 to 0.030 $Å^{-1}$ near the beam stop where the surface of the tactoids displays Porod behavior. For these close to 2D objects the surface scattering is dominated by the close to planar surface of the tactoids (verified by TEM). The Wilchinsky triangle (Fig. 6) shows that for both HD603 and

Table 2
Values of cosine square of angles made by scattering vector with MD, TD and ND in films HD603 and HD612. Bracketed values refer to WAXS values for the intercalated clay (002) reflection

Sample	HD603			HD612		
	$\langle\cos^2\phi_M\rangle$	$\langle\cos^2\phi_N\rangle$	$\langle\cos^2\phi_T\rangle$	$\langle\cos^2\phi_M\rangle$	$\langle\cos^2\phi_N\rangle$	$\langle\cos^2\phi_T\rangle$
Clay tactoids SAXS	0.078	0.770	0.152	0.122	0.712	0.166
Intercalated clay platelets (002) SAXS (WAXS)	0.094 (0.088)	0.812 (0.832)	0.094 (0.080)	0.057 (0.128)	0.877 (0.770)	0.066 (0.102)
Unmodified clay platelets (002) WAXS	0.131	0.594	0.275	0.136	0.474	0.390
Clay (110)/(020) plane WAXS	0.226	0.435	0.339	0.138	0.310	0.552
Polymer lamellae (001) SAXS	0.814	0.120	0.066	0.808	0.097	0.095
Polymer (110) unit cell plane WAXS	0.087	0.507	0.406	0.111	0.400	0.489

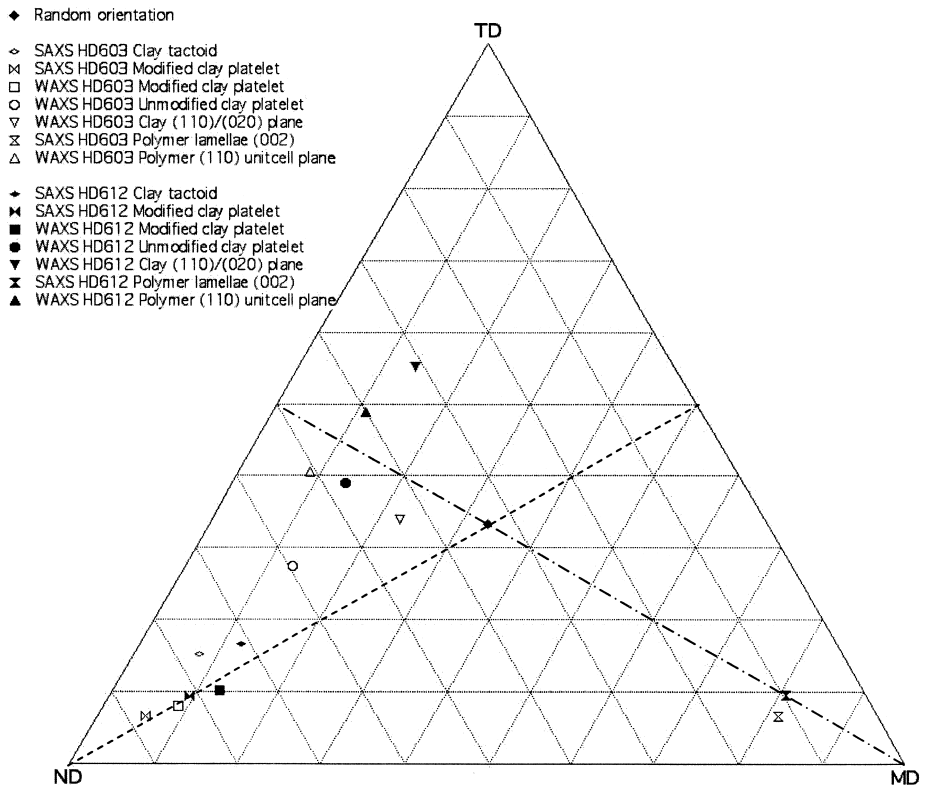

Fig. 6. Wilchinsky triangle [29–32] for average normal orientation of clay tactoids, unmodified clay platelets, intercalated clay platelets, clay (110)/(020) plane, polymer lamellae (001) and polymer (110) unit cell plane of HD603 and HD612 examined here. For a completely random oriented sample a point in the center results. (- - -) Points on this line have their normals randomly arranged in a MT projection. Proximity to ND reflects coplanarity with the MT plane. (–·–·–) Points on this line have their normals randomly arranged in the NT projection. Proximity to MD reflects coplanarity with the NT plane.

HD612, the clay tactoids (~0.12 μm) (a) lie with their normal (peak intensity) strongly oriented along the film normal direction (horizontal diamond in Fig. 6). These tactoids orient with the shear field in the film MT plane.

The SAXS radial plot (Fig. 3(a)) for the organically modified clay used in this study shows a peak at $q = 0.26$ Å^{-1} ($d = 24.2$ Å) indicating the presence of modified clay platelets in the clay used. In the radial plot for HD603 this clay peak shifts to $q = 0.228$ Å^{-1} ($d = 27.5$ Å). The increase in clay d-spacing from 24.2 to 27.5 Å indicates intercalation of a small amount (~13 vol%) of polymer (maleated PE) into the clay galleries. Increasing the compatibilizer concentration from 3% in HD603 to 12% in HD612 further increases the d-spacing to 31.4 Å indicating separation and intercalation of ~30 vol% expansion from the original modified clay. Thus the concentration of the compatibilizer has a strong effect on the intercalation and exfoliation of the modified clay platelets.

Unmodified clay is present at about 1/3 of the clay from integration of the radial plots. Thus ~4 wt% of the composite is intercalated clay. Assuming the density of both HDPE and maleated PE to be ~0.95 g/cc and the density of clay to be ~0.22 g/cc (data obtained from Southern Clay Products); the volume fractions of the polymer and clay in both the nanocomposite films are calculated in Table 3. The volume fraction numbers indicate that the ~13 and ~30% increase in clay volume on intercalation can be accounted for by part of the maleated PE intercalating with the clay. That is, it is possible that no pure PE chains enter the clay gallery. Further, it is necessary that some of the polyethylene blocks of maleated PE enter the clay gallery since there is insufficient volume of maleic blocks (2% of the maleated PE) to account for the observed volume change of the clay galleries.

For both HD603 and HD612 (with compatibilizer content of 3 and 12%, respectively), the intercalated/modified clay platelets, (b), lie with their normal strongly oriented along the film normal direction (squares and horizontal double triangles in Fig. 6) resulting in a point near the ND corner of the Wilchinsky triangle. This is consistent with the studies made earlier [17,18,20]. The orientation of modified/intercalated clay platelets is parallel to the orientation of clay tactoids (diamonds in Fig. 6), which could be an indication that the clay tactoids are composed of stacks of modified/intercalated clay platelets and these tactoids orient with the shear field in the film MT plane. The intercalated clay platelet normals in HD603 have slightly stronger orientation along ND as compared to HD612. Thus an increase in the compatibilizer concentration decreases orientation of the intercalated clay platelet

Table 3
Composition of the three films based on their densities. Concentration of intercalated clay is considered to be ~4 wt% in both the nanocomposite films. Increase in intercalated clay volume is based on ~13 and ~30% increase in its volume

SAMPLE	HDPE (density ~ 0.95 g/cc) (vol. fraction)	Maleated PE (density ~ 0.95 g/cc) (vol. fraction)	Intercalated clay (density ~ 0.22 g/cc) (vol. fraction)	Excess volume fraction[a] of the intercalated clay (vol. fraction)
HD000	1	0	0	0
HD603	0.818	0.027	0.155	0.020
HD612	0.737	0.108	0.155	0.047

[a] Excess volume fraction is function of total sample volume associated with expansion of clay galleries in the presence of maleated PE.

normals along the normal direction of the film mimicking the effect on tactoids.

The intercalated clay platelets can be seen in both, SAXS and WAXS, Fig. 2(b), so they serve as a comparison of the orientation values from the two detectors. Fig. 6 shows qualitative agreement as discussed above (horizontal double triangles and squares). WAXS is expected to show weaker orientation due to wavelength smearing and an estimate for the extent of WAXS smearing can be gained from the modified clay points (Fig. 6, squares).

As mentioned above, the radial plot for both nanocomposite films exhibit a peak at $q = 0.51$ Å^{-1} reflecting the presence of unmodified clay. The unmodified clay represents about one-third of the integrated intensity of the total clay. The concentration of the compatibilizer has no effect on the layer spacing of unmodified clay platelets. These platelets did not intercalate on addition to the polymer. While the modified/intercalated clay (b) shows strong orientation in the MT plane, the unmodified clay platelets (c) (circles in Fig. 6) lie basically with the M axis on the platelet plane but are arranged close to randomly in the NT plane (from a projection from M to the NT axis in the Wilchinsky triangle). Fig. 7(a) and (b) and b schematically shows the orientation of the modified/intercalated and the unmodified clay platelets with respect to the three film axes. From the Wilchinsky triangle it is clear that the normal to the unmodified clay patelets in HD612 is somewhat equally oriented along both film transverse and normal direction. Comparison of $\cos^2 \phi_N$, $\cos^2 \phi_T$ and $\cos^2 \phi_M$ values for the unmodified clay platelet normals in HD603 and HD612 from Table 2 indicates that the orientation of the unmodified clay platelet normal along the film normal direction decreases in HD612 as compared to HD603 (Fig. 6, circles). It is almost random in the NT plane.

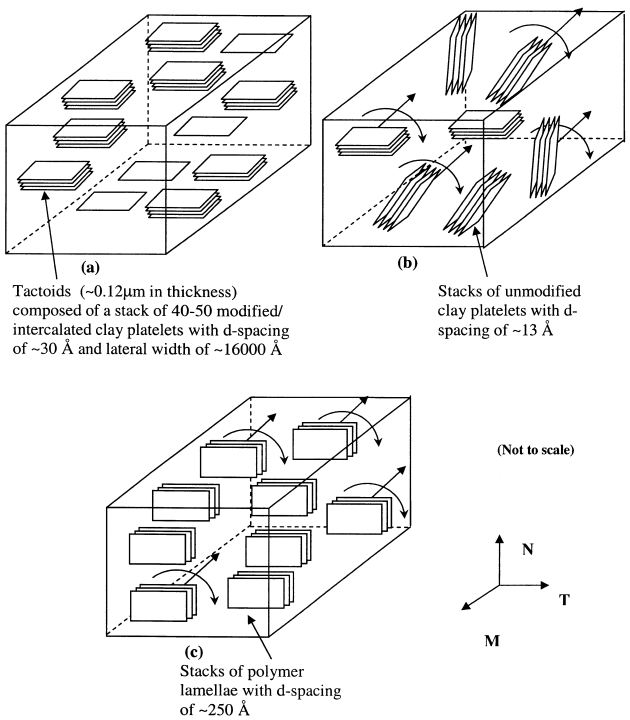

Fig. 7. Schematic of the orientation of (a) tactoids of modified/intercalated clay platelets, (b) unmodified clay platelets, and (c) polymer crystalline lamellae in the nanocomposite films.

In terms of orientation the intercalated clay platelets (b) are less dispersed (randomized) than the unmodified clay platelets (c) possibly due to an association with large size clay tactoids (a). This differs from the conventional view that tactoids are associated with unmodified clay.

Increase in concentration of the compatibilizer reduced ND orientation in the NT plane for the normal of the clay layers (Fig. 7). This could be an indication of a decrease in mobility due to viscosity changes for the clay layers on increase in compatibilizer concentration, as supported by the MI numbers in Table 1.

A combined reflection from the clay (110) and (020) planes (Fig. 6, inverted triangles) was observed in the 2D WAXS pattern (Fig. 2(b) and (d)). This clay in-plane reflection is observed in the X-ray diffraction pattern at $2\theta = 19.7°$ [12,13]. Since both (110) and (020) planes are perpendicular to the (001) plane of the clay platelet, the (110) and (020) plane reflection should be orthogonal to the (001) clay platelet reflection in the 2D WAXS patterns. However, the reflections are presumably a combination of unmodified and modified clay as well as both the (110) and (020) reflections so little orientation information is expected. The Wilchinsky plot shows that in the film NT plane, the clay (110)/(020) plane normals (inverted triangles, Fig. 6) in HD603 are equally oriented along both ND and TD, while in HD612 they are more oriented along TD.

The polymer lamellar crystals display a long period

reflection in SAXS and in plane (110) and (200) reflections in WAXS. The polymer chains in a polymer lamellar crystal c-axis are expected to be tilted at 34.4° to the lamellar normal [35]. If the polymer crystal orientation is governed by the lamellar orientation then a dispersion of crystallographic orientation in the (110) and (200) direction is expected due to the chain tilt. The alternative is crystal orientation controlled by chain orientation where the unit cell orientation would be higher than the lamellar orientation. For the HDPE films studied here, lamellar orientation is much stronger than crystallographic orientation (squares and vertical double triangle, Fig. 4(b)), so it can be said that the lamellar orientation governs the final polymer crystalline orientation. The chain tilt on average is randomly distributed about the lamellar normal for this case so on average, (001) is the same direction as the long-period. The 2D WAXS pattern for both HD603 and HD612 in MN orientation (Fig. 2(b), left face) shows that the average normal to the polymer unit cell (110) plane is oriented along the N direction of the film. In the MT orientation (Fig. 2(b), top face) this average normal orients along the T direction of the film. Calculating the angles made by the average normal of the (110) plane to the three film directions and plotting the Wilchinsky triangle shows that these average normals are close to randomly oriented in the NT plane. The Wilchinsky triangle (Fig. 6, triangles) shows that the average normal of the (110) plane is somewhat equally oriented in both the N and T direction of the film (Fig. 7). As seen in Fig. 6, these average normals to the polymer unit cell (110) plane (f), in HD603 (Fig. 6, unfilled triangle) is oriented more towards ND as compared to that in HD612 (filled triangle). Thus a similar change in orientation is observed between HD603 and HD612 for unmodified clay platelets (circles), and polymer unit cells (triangles), which may be an indication of some kind of attraction or physical similarity between unmodified clay platelets and polymer crystallites. The unmodified clay platelets are generally normal to the polymer lamellae.

Melt index (MI) data in Table 1, indicates that the MI of the polymer decreases (increase in viscosity) on addition of clay and compatibilizer. Fig. 8 shows the behavior of complex viscosity as a function of dynamic shear rate for the two samples. At low shear rates percolation of the clay particles and perhaps rotational motion apparently leads to a rather dramatic increase in the viscosity of the melt for higher concentrations of compatibilizer. This increase in viscosity supports the possibility of the presence of some kind of interaction between the polymer and the clay platelets and/or intercalation and dispersion of filler. These viscosity effects may enhance clay platelet orientation in the film N direction.

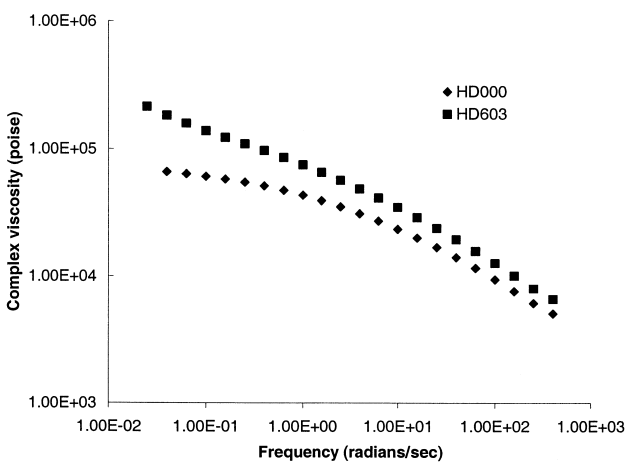

Fig. 8. Complex viscosity versus frequency for the three samples studied.

The SAXS radial plot (Fig. 3a) shows that the film HD000, with no clay, has a polymer lamellar peak at $q = 0.0296$ Å^{-1} ($d = 212$ Å). In the films HD603 and HD612 (with clay and compatibilizer) this polymer lamellae peak shifts to $q = 0.0245$ Å^{-1} ($d = 256$ Å) indicating an increase in the lamellar long period on addition of clay into the polymer regardless of the compatibilizer content and orientation variations. Earlier studies on the effect of nanoparticulate filler dispersion in polymers [1,35.36] observed a decrease in the polymer lamellae thickness on addition of the filler. They propose that the filler either acts as a nucleation site [36,37] or may physically hinder the growth of the lamellar structure [36] thus decreasing its thickness. Our observation of an increase in polymer lamellar period contrasts with these earlier studies. The dynamic cooling curves obtained from DSC (not shown) for the three films show a crystallization peak at almost the same temperature indicating no nucleation effect from the clay. The reason for this increase in lamellar thickness is unknown. The polymer melting point, heat capacity and the degree of crystallinity (78–80 wt%) of the films (Table 1), obtained from DSC, do not change significantly on addition of clay or compatibilizer. Apparently, the only factor that could affect the crystallization behavior is a change in surface energy (σ) of the polymer crystallites on addition of clay following the Gibbs–Thompson (Hoffman–Lauritzen) equation which predicts $l_c \sim \sigma$ (T_∞, T_c and ΔH_f remaining identical). One difference between this study and literature accounts is the observation of unmodified clay, which seems to have some association with the polymer lamellae in terms of orientation as discussed above. Such an association between unmodified clay and the growing polymer lamellae may lead to a modification of lamellar surface energy and a proportional change in lamellar thickness.

4. Conclusion

A technique to determine the 3D orientation of various hierarchical organic and inorganic structures in a polymer/layered-silicate nanocomposite (PLSN) was developed. The Wilchinsky triangle gives a clear and simple picture of the average orientation of various structural units with respect to the sample processing directions in a polymer–clay nanocomposite. This technique simplifies the

comparison and understanding of the effect of processing or composition variations on the orientation of various structures in a PLSN system. The effect of compatibilizer concentration on the orientation and dispersion of heirarchical components: clay tactoids, unmodified clay (001) plane normal, modified/intercalated clay (001) plane normal, clay platelet (110) and (020) plane normal, polymer lamellae (001) plane normal and polymer unit cell (110) and (200) plane normal in a PLSN system were studied.

Although the clay used in this study was organically modified, some unmodified clay platelets were observed along with modified clay platelets. In both HD603 and HD612 the modified/intercalated clay platelets were present as tactoids (thickness $\sim 0.12\,\mu m$ and lateral width $\sim 1.6\,\mu m$), which may be composed of a stack of around 40–50 clay platelets. For both HD603 and HD612, the clay tactoids lie with their normal strongly oriented along the film normal direction assuming a planar structure for the tactoids. These tactoids orient with the shear field in the film MT plane. For both HD603 and HD612, the unmodified clay platelets lie with their normal randomly oriented in the film NT plane. An increase in the compatibilizer concentration was found to reduce orientation of the normal to the unmodified clay platelets along the film N direction. Although an increase in compatibilizer concentration increased the layer spacing for the modified clay platelets, no increase in layer spacing for the unmodified clay platelets was observed.

The normal to the polymer unit cell (110) and (200) plane mimics the orientation of the normal to the unmodified clay platelets and the effect of the increase in compatibilizer concentration was similar on the unmodified clay and the unit cells. High compatibilizer loading was found to reduce the orientation of normals to both the unmodified clay platelets and the unit cells along the film N direction. This could be due to some kind of association or physical similarity between the unmodified clay platelets and polymer unit cells. The addition of clay was found to increase the polymer lamellar long period in the polymer–clay nanocomposites.

Thus, orientation data shows two surprising results. First tactoids are associated with intercalated clay and not with the unmodified clay. Secondly, the unmodified clay is associated with the polymer lamellae and may modify the lamellar surface energy.

By tuning clay platelet orientation we hope to control permeability and strength of polyolefin films. Orientation and dispersion are independent structural features, which must be simultaneously considered for the hierarchical structures present in PLSN's. Determination of dispersion in solid films (exfoliation) just by one projection can be misleading due to orientation of the same structures.

In the films studied, polymer lamellae and clay platelets are generally normal to each other. This may be due to different orientation forces acting on these plate structures. For polymer lamellae at high volume fraction, chain orientation prior to crystallization drives M direction orientation of lamellae normals in HDPE [38]. Finally it is the lamellae and not the chains which govern the final orientation of the polymer crystals since chain tilt leads to randomization of the unit cells and not the lamellar normals. For clay tactoids and platelets, shear forces during extrusion force orientation in the normal direction. Similar N direction orientation has been seen in LDPE where polymer lamellae orient in the N direction at low volume fraction of polymer crystallites [38]. This suggests that LDPE–clay nanocomposites may have some advantages over HDPE–clay nanocomposites.

Acknowledgements

The authors gratefully acknowledge Equistar Chemicals LP, Cincinnati, OH for providing the nanocomposite films. The authors also thank Mike Satkowski of Procter & Gamble Corporation, Cincinnati, OH for providing useful insight and discussions for this work. Use of the UNI-CAT beamline was possible through the gracious support of UNICAT. The UNICAT facility at the Advanced Photon Source (APS) is supported by the Univ. of Illinois at Urbana-Champaign, Materials Research Laboratory (US DOE, the State of Illinois-IBHE-HECA, and the NSF), the Oak Ridge National Laboratory (US DOE under contract with UT-Battelle LLC), the National Institute of Standards and Technology (US Department of Commerce) and UOP LLC. The APS is supported by the US DOE, Basic Energy Sciences, Office of Science under contract No. W-31-109-ENG-38. Equipment used in this project and G. Beaucage were supported by the National Science Foundation under grants CTS-9986656 and CTS-0070214.

References

[1] Jog J, Hambir S, Bulakh N, Kodgire P, Kalgaonkar R. J Polym Sci, Polym Phys 2001;39:446.
[2] Fornes T, Yoon P, Keskkula H, Paul D. Polymer 2001;42:9929.
[3] Oya A, Kurokawa Y, Yasuda H. J Mater Sci 2001;35:1045.
[4] Beyer G, Eupen K. Proceedings of the Nanocomposites. Chicago, IL, June 2001.
[5] Gilman J. App Clay Sci 1999;15:31.
[6] Kojima Y, Usuki A, Kawasumi M, Okada A, Karauchi T, Kamigaito O. J Appl Polym Sci 1993;49:1259.
[7] Messermith P, Giannelis E. J Polym Sci, Polym Chem 1995;33:1047.
[8] Brindley G, Brown G. Crystal structure of clay minerals and their X-ray identification. London: Mineralogical Society; 1980. p. 227–32.
[9] Alexander J, Dubois P. Mater Sci Engng 2000;28:1.
[10] Giannelis E, Krishnamoorti R, Manias E. Adv Polym Sci 1998;138:107.
[11] Vaia R, Fong H, Liu W, Wang C. Polymer 2002;43:775.
[12] Balazs A, Lyatskaya Y. Macromolecules 1998;31:6676.
[13] Takahashi S, Taniguchi M, Omote K, Wakabayashi N, Tanaka R, Yamagishi A. Chem Phys Lett 2002;352:213.
[14] Krishnamoorti R, Yurekli K. Curr Opin Colloid Interface Sci 2001;6:464.

[15] Varlot K, Reynaud E, Kloppfer M, Vigier G, Varlet J. J Polym Sci, Polym Phys 2001;39:1360.
[16] Varlot K, Reynaud E, Vigier G, Varlet J. J Polym Sci, Polym Phys 2002;40:272.
[17] Ogata N, Jimenez G, Kawai H, Ogihara T. J Appl Polym Sci 1997;64: 2211.
[18] Ogata N, Jimenez G, Kawai H, Ogihara T. J Polym Sci, Polym Phys 1997;35:389.
[19] Schmidt G, Nakatani A, Butler P, Karim A, Han C. Macromolecules 2000;33:7219.
[20] Kojima Y, Usuki A, Kawasumi M, Okada A, Karauchi T, Kamigaito O, Kaji K. J Polym Sci, Polym Phys 1994;32:625.
[21] Kojima Y, Usuki A, Kawasumi M, Okada A, Karauchi T, Kamigaito O, Kaji K. J Polym Sci, Polym Phys 1995;33:1039.
[22] Beaucage G, Aubert J, Lagasse R, Schaefer D, Rieker T, Erlich P, Stein R, Kulkarni S, Whaley P. J Polym Sci, Polym Phys 1996;34: 3063.
[23] Balsam M, Barghoorn P, Stebani U. Die Angewandte Makromolekulare Chemie 1999;267:1.
[24] González-Nuñez R, Padilla H, De Kee D, Favis B. Polym Bull 2001; 46:323.
[25] Yeh J-T, Chien-Cheng, Fan-Chiang, Yang S-S. J Appl Polym Sci 1997;64:1531.
[26] Wang KH, Choi MH, Koo CM, Choi YS, Chung IJ. Polymer 2001;42: 9819.
[27] Kodgire P, Kalgaonkar R, Hambir S, Bulakh N, Jog J. J Appl Polym Sci 2001;81:1786.
[28] Hasegawa N, Kawasumi M, Kato M, Usuki A, Okada A. J Appl Polym Sci 1998;67:87.
[29] Roe R. In: Methods of X-ray and Neutron Scattering in Polymer Science. New York: Oxford University Press, 2000. pp. 199.
[30] Bafna A, Beaucage G, Mirabella F, Skillas G, Sukumaran S. J Polym Sci, Polym Phys 2001;39:2923.
[31] Wilchinsky Z. J Polym Sci 1963;7:923.
[32] Alexander L. In: X-ray Diffraction Methods in Polymer Science. Florida: R. E. Krieger Publications, 1985, pp. 245.
[33] Beaucage G. J Appl Crystallogr 1995;28:717.
[34] Beaucage G, Aubect J, Lagasse R, Schaefer D, Rieker T, Eulich P, Stein R, Kulkarni S, Whaley P. J Polym Sci, Polym Phys 1996;34: 3063.
[35] Bassett D, Olley R, Alraheil I. Polymer 1988;29:1539.
[36] Lincoln D, Vaia R, Wang Z, Hsiao B, Krishnamoorti R. Polymer 2001;42:9975.
[37] Saujanya C, Radhakrisnan S. Polymer 2001;42:6723.
[38] Prasad A, Shroff R, Rane S, Beaucage G. Polymer 2001;42:3103.